Systems Analysis

SYSTEMS DIVISION

A. Some Periodic Orbits in the Rectilinear Restricted Three-Body Problem, *R. A. Broucke*

We have described in SPS 37-42, Vol. IV, pp. 31–33, and SPS 37-43, Vol. IV, pp. 20–22, some recent results obtained in the elliptic restricted three-body problem. The present article gives a few additional results relating to a special configuration of the elliptic problem: the case with equal masses and with extreme eccentricity $e = 1$. The two primaries are supposed to be moving in a Keplerian oscillatory motion on a straight line. This is the limit of the elliptic motion when the eccentricity tends to 1. We have first become aware of the interest of this problem when we have seen that some of the periodic orbits of Stromgren's problem can be extended all the way from the eccentricity $e = 0$ to the eccentricity $e = +1$. This leads us to the conclusion that a special study of the case $e = +1$ could be worthwhile. A similar conclusion was drawn in an article by J. Schubart (Ref. 1), in which he proposed to take the eccentricity $e = +1$ as a starting point to a systematic study of the elliptic restricted three-body problem.

We have used in this study a non-rotating inertial barycentric coordinate system. The equations of the motion of the satellite under the gravitational force of the primaries $(1 - \mu)$ and μ are

$$\frac{d^2x}{dt^2} = -(1-\mu)\frac{x - x_1}{r_1^3} - \mu\frac{x - x_2}{r_2^3},$$

$$\frac{d^2y}{dt^2} = -(1-\mu)\frac{y - y_1}{r_1^3} - \mu\frac{y - y_2}{r_2^3},$$

where the distances r_1, r_2 from the satellite to the primaries are given by

$$r_1^2 = (x - x_1)^2 + (y - y_1)^2,$$

$$r_2^2 = (x - x_2)^2 + (y - y_2)^2.$$

The coordinates of the two primaries are given by the well-known laws of elliptic motion. We have used them

in the form

$$x_1 = -\mu(-e + \cos E),$$
$$y_1 = -\mu(1 - e^2)^{1/2} \sin E$$
$$x_2 = (1 - \mu)(-e + \cos E),$$
$$y_2 = (1 - \mu)(1 - e^2)^{1/2} \sin E,$$

where the eccentric anomaly E is related to the time by Kepler's equation

$$t + X = E - e \sin E.$$

The phase constant X, in our application, may be taken equal to 0 or π according to the initial position of the primaries, either at pericenter or apocenter. Actually, all the orbits which will be described below belong to $X = 0$. There is no difficulty in the numerical solution of Kepler's equation even when $e = 1$. in order to describe the Keplerian motion of the two primaries as a function of time t. It is important to notice that the above formulation of the elliptic three-body problem is valid for all eccentricities ($0 \leq e \leq 1$). We shall consider here only the case $e = 1$. When we have the unit eccentricity, there is no sense anymore in using a rotating coordinate system for this problem, since the primaries are permanently moving on a non-rotating straight line. For the same reason the so-called Nechvile transformation cannot be applied when $e = 1$, and the simple form of the equations of motion, which is completely similar to the form for the circular case, cannot be used for high eccentricity.

Because of the straight-line motion of the two primaries, the problem that we are treating here presents some similarity with the well-known two-fixed center problem. Our problem may be considered as a generalization of it, the two "fixed centers" now moving on a straight line, according to Keplerian motion laws. Because of this fact, we have here a problem which seems more interesting than the two-fixed center problem: the problem we are studying is gravitationally consistent while the definition of the two-fixed center problem is somewhat arbitrary (the primaries attract the satellite but do not attract each other!). Among the similarities with the two-fixed center problem one can also mention the absence of the Coriolis force and the characteristic loops in the orbits, which are due to this force.

The numerical integration of the above equations of motion may encounter some difficulties due to the presence of the singularities $r_1 = 0$ or $r_2 = 0$. In this particular problem we have applied no regularization to the equations of motion.

Because of the simplicity of the equations of motion, we have first decided to integrate some orbits with regularly spaced initial conditions, in order to see if some periodic orbits would eventually exist. We have soon arrived at the rather surprising conclusion that a large number of periodic orbits are existing, although they are all isolated. We have then computed thirteen of these periodic orbits with somewhat higher precision. We have used the classical Runge-Kutta numerical integration procedure, with a variable step, equal to $0.005\, r_1 r_2$. Our objective was not mainly in the high precision of the numerical results, and for instance, by using full double precision, our end results have probably only five- or six-place accuracy. The periodic orbits have been obtained by two-dimensional linear differential corrections, once some good approximation had been obtained by the previous computer runs.

We have given in Fig. 1 a diagram which shows the initial conditions that have been explored. The initial conditions being of the form

$$(x_0, 0, 0, \dot{y}_0),$$

we have arbitrarily restricted ourselves to the limits

$$0.1 < x_0 < 1.0\,, \qquad 0.2 < \dot{y}_0 < 2.2\,.$$

We have also restricted the velocity $\dot{y}_0$ to be below some parabolic or escape velocity defined by

$$\dot{y}_0 = \left(\frac{2}{x_0}\right)^{1/2}.$$

Imposing all the above restrictions, we obtain the shaded area in Fig. 1. We have swept this area with regular intervals of 0.05 for x_0 as well as for $\dot{y}_0$. The thirteen points on this diagram correspond to the isolated periodic orbits which have been found. The eleven orbits three to thirteen form a single sequence: they all have one loop around one primary and an increasing number of loops around the other primary. We have given the initial conditions of the thirteen periodic orbits in Table 1. All thirteen orbits have the period $T = 2\pi$. In Fig. 2 we have shown the actual orbits, referred to the barycentric

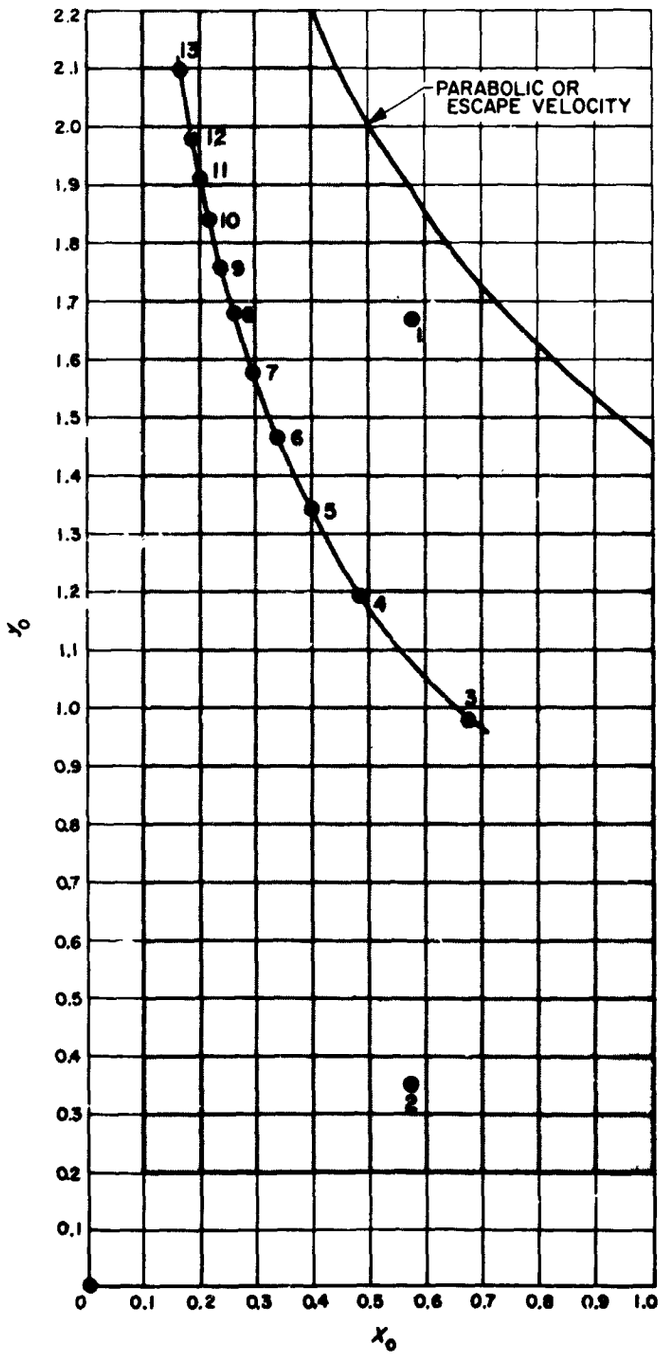

Fig. 1. Diagram of initial conditions for periodic orbits

coordinate system. In Fig. 3 we have shown the six most simple orbits referred to a coordinate system centered at one primary $m_1 = 1 - \mu$ (geocentric) and the other primary $m_2 = \mu$ (selenocentric). In our particular problem we have equal masses $1 - \mu = \mu = 1/2$, and we use the word "geocentric" for the coordinate system centered at the primary which is shown on the left side in our figures.

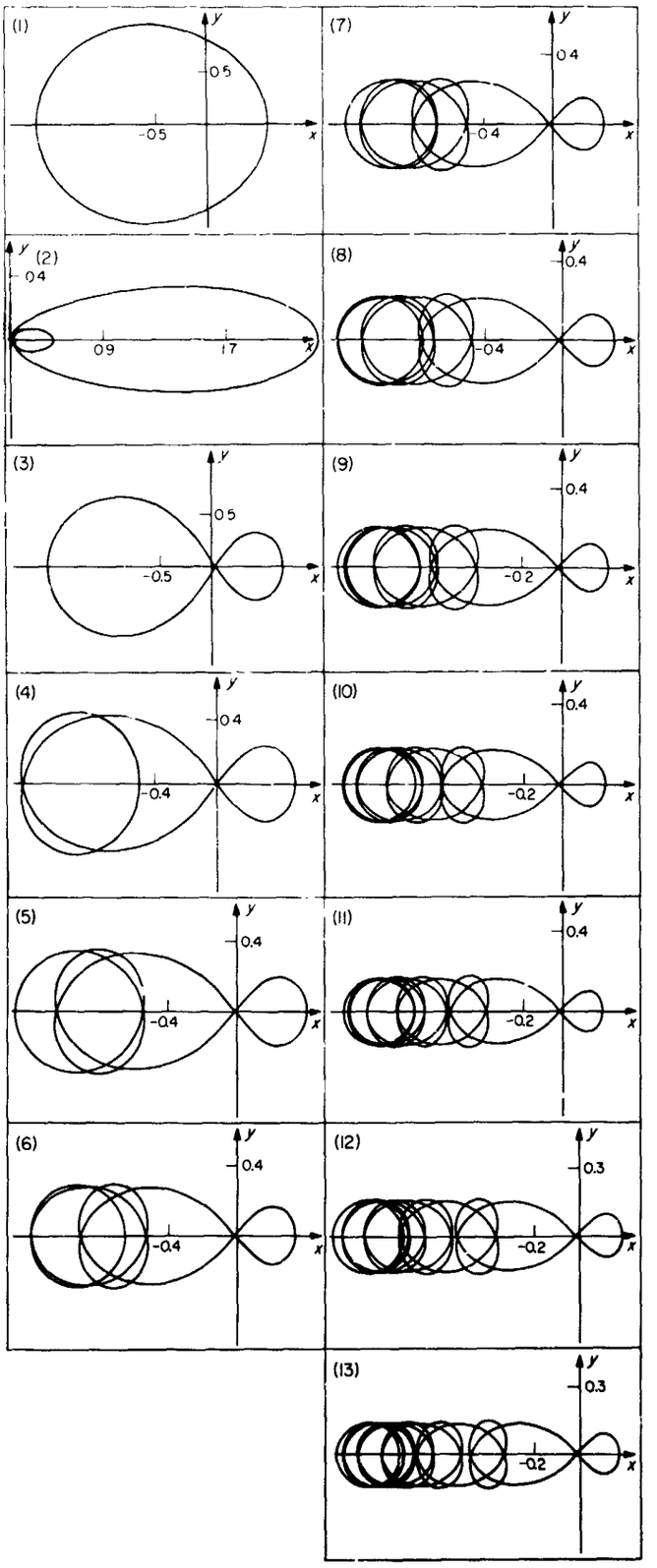

Fig. 2. The 13 periodic orbits in the barycentric (inertial) coordinate system

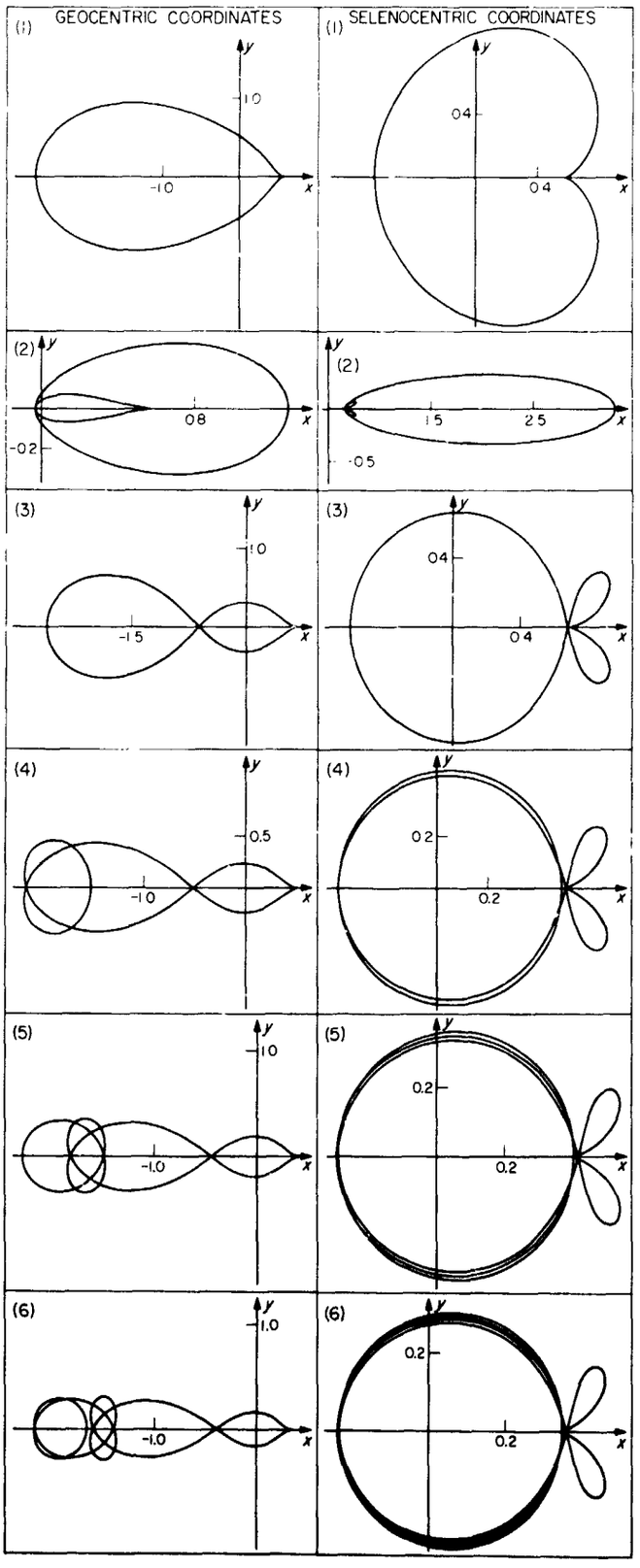

Fig. 3. The first 6 periodic orbits in the geocentric and the selenocentric coordinate systems

Table 1. Initial conditions for 13 periodic orbits

Orbit number	x_0	$\dot{y}_0$
1	0.579152	1.680050
2	0.574506	0.346101
3	0.682309	0.981417
4	0.492110	1.192088
5	0.396211	1.347039
6	0.336523	1.473383
7	0.295148	1.581601
8	0.264484	1.677079
9	0.240690	1.763014
10	0.221596	1.841481
11	0.205876	1.913916
12	0.192667	1.981358
13	0.171617	2.104198

Similarly, "selenocentric" refers to the primary shown on the right side. When we use the geocentric or selenocentric coordinates, we can see that some cusps are present in the form of the orbits. These cusps are due to accelerated translational motion of the frame of reference rather than the motion of the satellite.

As a matter of conclusion let us say that we have here thirteen isolated periodic orbits; however, these orbits are not isolated as far as e and μ are concerned. We have prepared a computer program which should generate new periodic orbits by varying e or μ in a more or less automatic way. For instance, we have been able to make the following computer runs:

(1) In the neighborhood of orbit 1: 22 periodic orbits with $e = 1.0$ and $\mu = 0.5$ to 0.479.

(2) In the neighborhood of orbit 2: 12 periodic orbits with $\mu = 1/2$ and $e = 1.0$ to 0.988; 26 periodic orbits with $e = 1.0$ and $\mu = 0.5$ to 0.458.

(3) In the neighborhood of orbit 3: 23 periodic orbits with $e = 1.0$ and $\mu = 0.5$ to 0.466.

B. *Mariner Mars 1969* Celestial Mechanics Experiment, *J. D. Anderson*

1. Summary

An error analysis has been performed for a set of 15 parameters determinable from the *Mariner Mars 1969* tracking data. Among these 15 parameters are the Earth-Moon mass ratio, the mass of Mars, the astronomical unit, and the position of Mars at spacecraft-Mars encounter.

It is these parameters which are of importance to the celestial mechanics experiment (CME), at least for tracking data taken within the mission duration of launch to encounter plus 3 months.

The motivation for the analysis is to determine the value of adding range data to the spacecraft tracking and to investigate the effect of gas jetting from the infrared spectrometer (IRS) during planetary encounter. The conclusion with respect to range data is that they significantly improve the value of the experiment. With range data it should be possible to determine the astronomical unit and the position of Mars to better than 100 m. Without range data this number is increased to about 1500 m, and realistically the error could be larger because of an inability to calibrate the charged particle contribution to the doppler signal. Both range and doppler data permit this calibration, and provide as well an improved opportunity for data validation.

If the uncertainty in the force imparted by the IRS gas jetting is less than ± 1 dyne over a 90-min period around encounter, then the effect on the CME is insignificant. For an uncertainty greater than ± 1 dyne it is necessary to include a model for the IRS jetting in the solution for the astronomical constants, particularly for the mass of Mars. With the inclusion of this model, we would attempt to reduce the uncertainty in the force from the IRS jetting to the level of ± 1 dyne. In order to accomplish such a reduction the *a priori* uncertainty should certainly not be greater than ± 100 dynes, a number two orders of magnitude larger than the ultimate goal of ± 1 dyne. The *a priori* uncertainty is defined as that obtained from preflight design and testing of the IRS gas jetting system and from any useful telemetry obtained during the jetting period.

2. Effect of Range Data on Celestial Mechanics Experiment

In Subsection 5, errors on the orbital parameters and astronomical constants are computed for doppler tracking data only and for doppler and range data. The results indicate the significance of adding ranging data as far as the celestial mechanics parameters are concerned. In a sense this is an extension of an earlier article (SPS 37-43, Vol. III, pp. 18–24) where the addition of range data to a single pass of tracking was considered. Of course it is an oversimplification to judge the value of ranging data solely on the basis of an error analysis of the sort given here. Other considerations, such as having an independent type of data to compare with the doppler measurements, are equally important. Perhaps more important, D. Trask and L. Efron (SPS 37-41, Vol. III, pp. 3–11) point out that a combination of doppler and range observations can be used to calibrate the total (ionosphere and space plasma) charged particle effect on both types of data. This is especially important for *Mariner 1969*, which does not include a dual frequency experiment. A. Liu and R. Motsch (SPS 37-44, Vol. III, pp. 28–33) have explored further the possibility of a charged particle calibration.

Nevertheless, with the limitations of the present analysis clearly in mind, it is possible to conclude that adding range data to the doppler tracking can reduce the uncertainty on the astronomical unit from a region of ± 150 to ± 1300 m with doppler data only to a region of ± 25 to ± 65 m for range and doppler data. The position of Mars is reduced from a region of ± 150 to ± 1700 m to a region of ± 15 to ± 90 m. The effects on uncertainties in the masses of the Moon and Mars are not as pronounced as for the astronomical unit and the position of Mars.

3. Effect of IRS Gas Jetting on Celestial Mechanics Experiment

In this article it is assumed that the gas jetting from the IRS experiment occurs in a period 1 hr before planetary encounter to ½ hr after encounter, a total period of 90 min. To see what this means in terms of a corruption of doppler and range data, consider the time variation in the geocentric radial velocity and range of the spacecraft during a 12-hr period centered about the encounter time. Fig. 4 shows a plot of the geocentric radial velocity and

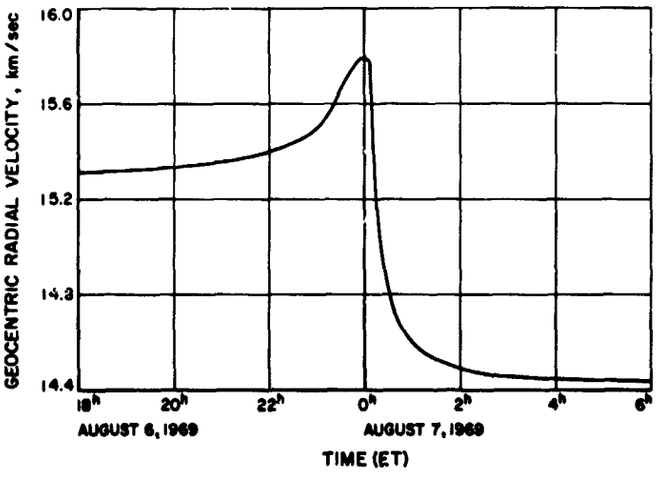

Fig. 4. Geocentric radial velocity vs time during planetary encounter

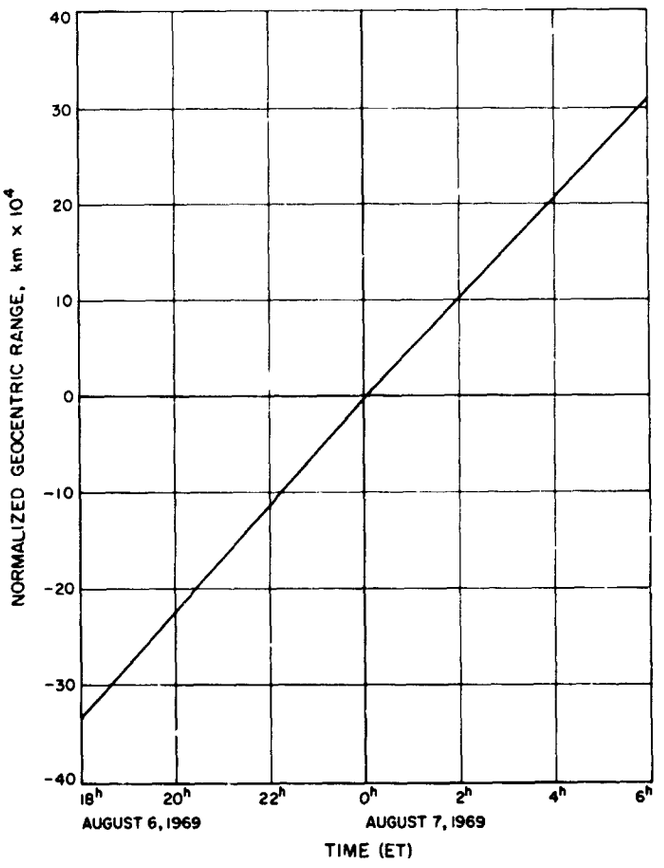

Fig. 5. Difference in geocentric range of date and geocentric range at planetary encounter vs time

Fig. 5 shows the difference between the geocentric range of date and the geocentric range at encounter. Now, as an extreme case, suppose that the tracking data during the 90 min of gas jetting are completely neglected in the determination of the constants. It is clear from Fig. 4 that a significant portion of the doppler curve is lost and that some sort of degradation will occur in the accuracy of constants which depend on the close approach to the planet for their determination. For example, the accuracy of the mass of Mars could easily be degraded. On the other hand, the time variation of the geocentric range during the encounter period does not exhibit any peculiarities during the 90 min of jetting, and the contribution of the range data to the determination of constants should not be significantly affected by the loss of data.

It is important to realize that the gas jetting affects the determination of the constants in two ways. The first and most straightforward is the introduction of a systematic source of error during the 90-min jetting period. This can be handled, as in Subsection 4, by assuming that the tracking data are corrupted by the jetting and by weighting the corrupted data less in the weighted least squares procedure. The other effect on the determination of the constants is that the orbit of the spacecraft is perturbed during the jetting period, and, as a result, when the gas is depleted, the orbit is not known as well as if the gas jetting had not occurred. This situation can also be handled by properly representing the statistics of the orbital parameters at the end of the gas jetting. Thus, orbital errors which result from the jetting are mapped into the errors in the constants as determined from data taken before, during, and after the jetting period.

Effects of the jetting on the orbital position after a period T can be estimated from $\frac{1}{2} FT^2/m$, which for a force F of 100 dynes amounts to 56 m, while the effect on velocity from FT/m is 0.02 m/sec for the same force. In this article, the inabilty to compute a perfectly accurate orbit because of an uncertainty in the force model during gas jetting is ignored, and the only effect of jetting on the orbit and constants is presumably to decrease the accuracy of the data during the jetting period.

The numerical results of Subsection 5 show that the only constant significantly affected by the gas jetting is the mass of Mars and that an uncertain force greater than ± 100 dynes effectively destroys the doppler data taken during the jetting period. Even at ± 10 dynes, over 90% of the potential information in the close encounter data is lost. The addition of range data during the jetting period reduces the ± 10-dyne effect on the mass from a 3σ degradation for doppler data only to a 2σ degradation for range and doppler data. In order that the gas jetting not seriously impair the solution for the mass, it is important that the random uncertainty on the force be considerably less than ± 10 dynes and that range data be taken during a significant portion of the jetting period. Ultimately, the force should be known to ± 1 dyne. A calibration for charged particle effects with range and doppler data is an important part of achieving this ultimate accuracy.

4. Gas Jetting as a Systematic Error Source[1]

Let gas escape from a spacecraft of mass m at a force level equal to F in dynes. Then the acceleration a imparted to the spacecraft is $a = F/m$, and if the force is

[1]The author wishes to thank D. W. Curkendall for assistance in preparing Subsection 4.

exerted over a time interval T, the deviation in the position of the spacecraft at the end of the interval, compared to a gas-free position, is $\Delta\rho = \frac{1}{2} aT^2$. Alternatively, suppose that counted doppler observations are obtained from which the change in topocentric range over some count time interval T_c is deduced. If the error in this range change is expressed in terms of an error $\sigma_{\dot\rho}$ in topocentric range rate, then the range change error over the count interval T_c is given by $T_c\,\sigma_{\dot\rho}$. Further, if the range error is accumulated over N samples of doppler data, then the integrated range error over the N samples is $T_c\,(N)^{1/2}\,\sigma_{\dot\rho}$, and for an even distribution of samples over the time interval T, such that $T = NT_c$, the integrated range error is $(TT_c)^{1/2}\,\sigma_{\dot\rho}$.

The approach followed here, in representing the error from an unknown gas jetting force, is to absorb the systematic error from the gas jetting into N independent range rate measurements. All that is required is to equate the range error $\frac{1}{2} aT^2$ from the gas jetting over the time interval T to the integrated range error $(TT_c)^{1/2}\,\sigma_{\dot\rho}$ over the same time interval. The resulting range rate error for N independent samples at intervals T_c is

$$\sigma_{\dot\rho} = \frac{1}{2}\,\frac{F}{m}\left(\frac{T^3}{T_c}\right)^{1/2} \tag{1}$$

Let the gas jetting occur over a period of 90 min and set $m = 259$ kg and $T_c = 1$ min. Then for F given in dynes the numerical expression of Eq. (1) is

$$\sigma_{\dot\rho} = 0.0989\,F \text{ cm/sec} \tag{2}$$

The accuracy of the doppler data is conservatively rated at 0.1 cm/sec when sampled at 1-min intervals, and thus it is apparent from Eq. (2) that if the unknown force F is greater than ± 1 dyne, the gas jetting can be considered a serious source of error. One of the purposes of this article is to investigate fairly rigorously the implications of an unknown force of greater than 1 dyne, at least as far as celestial mechanics parameters are concerned.

5. Numerical Results

A version of the JPL orbit determination program (SPODPA—Mod II, program tape 9493) is used to obtain variances on various constants and parameters of astronomical interest. The orbital parameters for the spacecraft are represented by geocentric equatorial coordinates at the epoch, the position of Mars by heliocentric cartesian coordinates at the time of the spacecraft's planetary encounter, the mass of the Moon by the selenocentric gravitational constant GM, the Martian gravitational constant by the mass of Mars in solar mass units, and the astronomical unit A is given in metric units. Actually, the fundamental unit is light seconds in the determination of the astronomical units, but error estimates are often given in metric units. The non-gravitational parameters γB, GT and GN are also included in the parameter statistics to allow for uncertainties caused by solar radiation pressure and attitude control forces. The uncertainties for these three parameters are given as a percentage of the total solar radiation pressure. Their inclusion as deterministic parameters results in realistic uncertainties only if the actual *Mariner 1969* data are reduced with an estimator designed to handle random time varying forces.

All error estimates are obtained for two extremes in assumed station location error. The first assumes no error and the second ± 5 m in station location uncertainties. Note that Hamilton, Grimes, and Trask (SPS 37-44, Vol. III, pp. 4–11) have stated that a goal of ± 1 m uncertainty in station locations is reasonable for *Mariner 1969* data reduction. By using ± 0 and ± 5 m, the region of uncertainty for the parameters should be conservatively defined.

Other numerical data which go into a computation of the uncertainties are given in Table 2.

The resulting errors in the 15 parameters of a simulated least squares solution are obtained from the covariance matrix computed in SPODPA—Mod II. In Table 3 the standard deviations are given with no IRS gas jetting during encounter. Four solutions are represented to demonstrate the advantage of including range data. They are:

Solution	Type of data
A	Range and range-rate data, no station location error
B	Range-rate data, no station location error
C	Range and range-rate data, ±5-m station location error
D	Range-rate data, ±5-m station location error

When IRS gas jetting errors are included, by the method of Subsection 4, there is no appreciable effect on any of the

Table 2. Data used in the computation of uncertainties

Geocentric true equatorial coordinates (March 18, 1969, 11^{h}52^{m}43^s.000 ET)	
x, km	−5105058.17
y, km	−1140554.5
z, km	−1118697.0
$\dot{x}$, km/sec	−1.6423604
$\dot{y}$, km/sec	−2.1007967
$\dot{z}$, km/sec	−2.0376762
Heliocentric osculating elements referred to true ecliptic and equinox (August 3, 1969, 13^{h}30^{m}48^s.319 ET)	
a, km	1119835290
e	0.22207465
T	February 26, 1969, 00^{h}03^{m}4^s.069 ET
i, deg	1.7830771
Ω, deg	351.34975
ω, deg	164.38212
Aerocentric osculating elements referred to true ecliptic and equinox (August 7, 1969, 00^{h}00^{m}53^s.541 ET)	
a, km	−953.33386
e	6.7704032
T	August 7, 1969, 00^{h}00^{m}53^s.541 ET
i, deg	15.817714
Ω, deg	246.27758
ω, deg	297.13641
Additional parameters	
Astronomical unit, km	149598500
Sun–Mars mass ratio	3088000
Epoch for position of Mars	August 7, 1969, 00^{h}00^{m}35^s.000 ET
Assumed doppler error	±1 mm/sec random range rate error at 1-min sample interval
Assumed range error	±367.4-m random range error at 1-min sample interval (this corresponds to one range measurement per 10-hr tracking pass with an uncertainty of 367.4/(600)$^{1/2}$ or 15 m)
Duration of tracking (continuous coverage)	March 19, 1969, 0^{h}0 to November 7, 1969, 0^{h}0
A priori error on parameters	
(x, y, z), km	10^8
$(\dot{x}, \dot{y}, \dot{z})$, km/sec	1.0
$(x_\delta, y_\delta, z_\delta)$, km	500
GM, km^3/sec^2	0.2
M_δ, ppm	16.63
A, km	500
(γB, GT, GN), %	1.0

Table 3. Standard deviations in the absence of IRS gas jetting

Parameter	No station location error		±5-m station location error	
	ρ and $\dot{\rho}$ (A)	$\dot{\rho}$ only (B)	ρ and $\dot{\rho}$ (C)	$\dot{\rho}$ only (D)
x, m	24	128	188	1054
y, m	31	91	517	2048
z, m	25	77	383	1984
$\dot{x}$, μ/sec	4	27	14	284
$\dot{y}$, μ/sec	3	12	29	188
$\dot{z}$, μ/sec	3	17	23	132
x_δ, m	9	42	68	131
y_δ, m	14	154	33	1658
z_δ, m	7	59	87	647
GM, km^3/sec^2	0.000056	0.000169	0.000399	0.000255
M_δ, ppm	0.24	0.25	1.03	0.48
A, m	26	150	65	1312
γB, %	0.000231	0.00142	0.00102	0.0179
GT, %	0.000381	0.00300	0.00565	0.0394
GN, %	0.000268	0.00130	0.00349	0.00518

Table 4. Standard deviation in ppm for the mass of Mars at various levels of IRS gas jetting uncertainty

Uncertainty in IRS force, dyne	No station location error		±5-m station location error	
	ρ and $\dot{\rho}$ (A)	$\dot{\rho}$ only (B)	ρ and $\dot{\rho}$ (C)	$\dot{\rho}$ only (D)
No force	0.24	0.25	1.03	0.48
±10	0.55	0.74	5.96	1.51
±100	0.57	0.78	6.39	1.72
±500	0.57	0.78	6.39	1.72

15 parameters except the mass of Mars. In Table 4 the results for the mass are given as standard deviations in parts per million of the total mass. Again the four solutions (A, B, C, D) are represented.

C. A Distribution Free Method Involving the Spacing of Independent Sample Points, *H. Lass*

Consider a continuous probability density function (PDF), $p(x)$, with $p(x) \geqq 0$ and $\int_{-\infty}^{\infty} p(x)dx = 1$. An interesting problem whose solution is well known is the following. What is the probability that from n independent samples the proportion of the population between the minimum and maximum values of the sample data will exceed β, $0 < \beta < 1$?

To solve this problem, we note that if $z = \int_{-\infty}^{x} p(t)dt$ then z is a random variable whose PDF is uniform on the interval [0, 1], since $0 \leqq z \leqq 1$ for all x and $q(z)dz = p(x)dx$, which implies that $q(z) = 1$ from $dz/dx = p(x)$ wherever $p(x)$ is continuous. From

$$\int_{x_{min}}^{x_{max}} p(t)dt = \int_{-\infty}^{x_{max}} p(t)dt - \int_{-\infty}^{x_{min}} p(t)dt = z_2 - z_1 \quad (1)$$

we recognize that we need only solve the problem for a uniform PDF on [0, 1]. Let u and v be the minimum and maximum values, respectively, from n sample values obtained from a uniform PDF. The joint density function on (u, v) is simply

$$p(u, v) = n(n-1)(v-u)^{n-2} \quad (2)$$

since there are n choices for u, $(n-1)$ choices for v, while the remaining $(n-2)$ sample values must lie between u and v with probability $(v-u)^{n-2}$. Hence

$$\text{Prob}\,(z_2 - z_1 \geqq \beta) = \int_0^{1-\beta} \int_{u+\beta}^{1} n(n-1)(v-u)^{n-2}\,dv\,du$$
$$= 1 - \beta^n - n\beta^{n-1}(1-\beta) \quad (3)$$

If we desire that Prob $(z_2 - z_1 \geqq \beta) = \alpha$, then $1 - \beta^n - n\beta^{n-1}(1-\beta) = \alpha$, which enables one to find the number of sample values, n, for fixed α, β. Thus 93 sample data are needed if we desire that the proportion of the population between the extreme values of the data exceed 95% ($\beta = 0.95$) with probability $\alpha = 0.95$.

Now the above analysis tells us little, if anything, about the spacing of the sample data between the extreme values of the data. Let us impose the condition that

$$\text{Prob}\left[\int_{y_i}^{y_{i+1}} p(t)dt \leqq \alpha\right] \qquad i = 1, 2, \cdots, n-1 \quad (4)$$

with $y_1 < y_2 < \cdots < y_i < y_{i+1} < \cdots < y_n$, the ordered statistics. Again we need only consider the problem by dealing with the uniform PDF on [0, 1].

The density function for the ordered statistics is

$$p(y_1, y_2, \cdots, y_n) = n!, \qquad 0 \leqq y_1 \leqq y_2 \leqq \cdots \leqq y_n \leqq 1 \quad (5)$$

since there are n choices for y_1, $(n-1)$ choices for y_2, etc. We consider the transformation

$$\begin{aligned} y_1 &= z_0 \\ y_2 &= z_0 + z_1 \\ y_3 &= z_0 + z_1 + z_2 \\ &\vdots \\ y_n &= z_0 + z_1 + z_2 + \cdots + z_{n-1} \end{aligned} \quad (6)$$

whose Jacobian is identically one, so that the joint density function on $z_0, z_1, \cdots, z_{n-1}$ is

$$q(z_0, z_1, z_2, \cdots, z_{n-1}) = n! \quad (7)$$

with $z_i \geqq 0$, $0 \leqq \sum_{i=0}^{n-1} z_i \leqq 1$, since $z_0 = y_1$, $z_1 = y_2 - y_1$, $z_2 = y_3 - y_2, \cdots, z_{n-1} = y_n - y_{n-1}$.

Since we are interested in the random variables $z_1, z_2, z_3, \cdots, z_{n-1}$, we integrate out the random variable z_0 to obtain

$$h(z_1, z_2, \cdots, z_{n-1}) = n!\ (1 - z_1 - z_2 \cdots - z_{n-1}) \quad (8)$$

with $z_i \geqq 0$ and $\sum_{i=1}^{n-1} z_i \leqq 1$. Thus

$$P_n(\alpha) \equiv \text{Prob}\,(z_1 \leqq \alpha, z_2 \leqq \alpha, \cdots, z_{n-1} \leqq \alpha)$$
$$= n! \int_0^{\alpha} \int_0^{\alpha} \cdots \int_0^{\alpha} (1 - z_1 - z_2 \cdots - z_{n-1})$$
$$U(1 - z_1 - z_2 \cdots - z_{n-1})dz_1 \cdots dz_{n-1} \quad (9)$$

with $U(\xi)$ the unit step function, $U(\xi) = 0$ for $\xi < 0$, $U(\xi) = 1$ for $\xi \geqq 0$.

Let $k\alpha + \gamma = 1$ with $0 \leqq \gamma < \alpha$ so that k is the largest integer for which $k\alpha \leqq 1$. Successive integrations of Eq. (9) yield

$$P_n(\alpha) = \sum_{r=0}^{k} (-1)^r \binom{n-1}{r} (1 - r\alpha)^n \quad (10)$$

If, for example, $n = 4$, $\alpha = \frac{1}{3}$, we have $k = 3$ and $P_4(\frac{1}{3}) = \frac{13}{27}$.

The author has been unable to find a closed form for $P_n(\alpha)$. However, a computer should enable one to evaluate $P_n(\alpha)$ for various values of α and n.

D. Techniques for Studying Dispersions of Nonlinear Systems, *S. R. McReynolds*

Let X be a continuous ensemble of vector objects $\{x^i\}$ with an initial known density function $p_0(x)$. Suppose that each object satisfies a set of nonlinear differential equations

$$\dot{x}_j = f^j(x, t) \qquad (j = 1, n) \tag{1}$$

Then an important engineering question is to find the density function $P(x, t)$ of x at a future time t. In general, this task is impossible from an analytic standpoint and laborious from a computational standpoint. In this article we concern ourselves with techniques that may be used to determine quantitative characteristics of $P(x, t)$.

1. The Continuity Equation

Elementary consideration, such as that employed in fluid mechanics, leads us at once to a partial differential equation for $P(x, t)$:

$$\frac{\partial P}{\partial t} + \sum_i \frac{\partial}{\partial x_i}(Pf^i) = 0 \tag{2}$$

This equation is referred to as the "continuity equation," and is a special case of the Fokker-Planck equation.

2. Solution by Characteristics

Eq. (2) is a quasi-linear, first-order partial differential equation. Together with the initial density function $P_0(x)$ the solution may be computed numerically. To avoid the problem of computing the partials of P with respect to x by differencing, one may employ the use of characteristics.

In this case, the characteristics consist of the trajectories that the objects follow, namely, solutions to the ordinary set of equations $\dot{x} = f(x, t)$. Along these characteristics the derivative of P, which we denote as $\dot{P}$, is given by

$$\dot{P} = -P \sum_i \frac{\partial f^i}{\partial x_i} \tag{3}$$

The solution to this differential equation is given by

$$P(T) = P_0 \exp\left[-\int_0^T \sum_i \frac{\partial f^i}{\partial x_i} dt \right] \tag{4}$$

The method of solution proceeds as follows. Partition the set of initial conditions by selecting points in the region of interest. Map these initial points forward by integrating the system equations until time T. The probability density of the ensemble at this point is given by Eq. (4), where the integral is along the corresponding trajectory

Eq. (4) indicates the relationship between stability and diffusion of densities. We note that $\sum_i \partial f^i/\partial x_i$ = trace $(\partial f^i/\partial x_i)$ = the sum of real parts of eigenvalues of $(\partial f^i/\partial x_i)$. If the system is stable, the real parts of the eigenvalues are negative, and hence $\sum_i \partial f^i/\partial x_i < 0$. Thus, as indicated by Eq. (4), the density of objects will increase with the time along such a trajectory. On the other hand, if the system is unstable, then $\sum_i \partial f^i/\partial x_i > 0$, and the density will decrease with time along the trajectory.

Example:

$$\dot{x} = \epsilon x, P_0(x) = \begin{cases} \frac{1}{2}, & |x| \leq 1 \\ 0 & |x| > 1 \end{cases}$$

$$P(x, T) = \begin{cases} \frac{1}{2}e^{-\epsilon T} & |x| \leq e^{+\epsilon T} \\ 0 & |x| > e^{\epsilon T} \end{cases}$$

Some systems have the property that $\sum_i \partial f^i/\partial x_i = 0$. For these systems the probability densities remain constant along a trajectory. An important example of this is Hamiltonian systems. Hamiltonian systems are systems which satisfy

$$\dot{p}_i = \frac{\partial H}{\partial q_i}\,; \quad \dot{q}_i = \frac{-\partial H}{\partial p_i} \quad (i = 1, n)$$

Obviously $\sum_i \partial f^i/\partial x_i = \sum_i (\partial H/\partial p_i\, \partial q_i - \partial H/\partial q_i\, \partial p_i) = 0$. Conservation of probability density for Hamiltonian systems is known in classical mechanics as Liouville's theorem.

3. A Functional Approximation Technique

For many important cases the initial density is Gaussian

$$P_0(x) = Ke^{-\frac{1}{2}||x-\bar{x}_0||_S^2} \tag{5}$$

S here is a positive semi-definite matrix, and $||x-\bar{x}_0||_S^2$ is the quadratic form $(x-\bar{x}_0)^T S(x-\bar{x}_0)$ (T denotes transposition). From Eq. (3), it is clear that $P(x,t)$ has the form

$$P(x,t) = K e^{-L(x,t)} \tag{6}$$

Now by substituting this into Eq. (2), it is seen that $L(x,t)$ satisfies the partial differential equation

$$\frac{\partial L}{\partial t}(x,t) + \sum_i \frac{\partial L}{\partial x_i}(x,t) f^i(x,t) = r(x) \tag{7}$$

where

$$r(x) = \sum_i \frac{\partial f^i}{\partial x_i}(x,t) \tag{8}$$

The initial boundary condition for $L(x,t)$ is given by

$$L(x,t_0) = -\frac{1}{2}||x-\bar{x}_0||_S^2 \tag{9}$$

The functional technique we shall suggest here consists of approximating $L(x,t)$ in the neighborhood of a trajectory (characteristic) with a quadratic form.

Let a nominal trajectory $\bar{x}(t)$ be chosen as follows:

$$\begin{aligned} \bar{x}(0) &= x_0 \\ \dot{\bar{x}}_i &= f^i(\bar{x},t) \end{aligned} \tag{10}$$

Now along this trajectory, differential equations (characteristic equations) may be derived for the partial derivatives of $L(x,t)$ with respect to x. These are obtained by taking the partial derivatives of Eq. (7) with respect to x. The first partial derivative of Eq. (7) with respect to x_j, evaluated at $\bar{x}$, yields

$$\frac{\partial}{\partial t}\frac{\partial L}{\partial x_j} + \sum_i \frac{\partial}{\partial x_i}\frac{\partial L}{\partial x_j} f^i(\bar{x},t) + \sum_i^n \frac{\partial L}{\partial x_i}\frac{\partial f^i}{\partial x_j}(\bar{x},t) = \frac{\partial r}{\partial x_j}(\bar{x},t) \tag{11}$$

Now we note that the operator $\partial/\partial t(\ ) + \sum_i \frac{\partial}{\partial x_i}(\ ) f^i(\bar{x},t)$ is the total derivative operator along the characteristic $\bar{x}(t)$. Denoting this operator by $(\dot{})$, Eq. (11) becomes

$$\frac{\partial \dot{L}}{\partial x_j} = -\sum_i \frac{\partial L}{\partial x_i}\frac{\partial f^i}{\partial x_j}(\bar{x},t) + \frac{\partial r}{\partial x_j}(\bar{x},t) \tag{12}$$

Note that from Eq. (9),

$$\frac{\partial L}{\partial x_j} = -(x-\bar{x}_0)\Big|_{x=\bar{x}(0)} = 0 \tag{13}$$

Hence Eqs. (12) and (13) may be used to compute $\partial L/\partial x_j$ along the characteristic x.

To obtain the characteristic equation for $\partial^2 L/\partial x_j \partial x_k$, the partial derivative of Eq. (11) is taken with respect to x_k. This results in

$$\begin{aligned} &\frac{\partial}{\partial t}\frac{\partial^2 L}{\partial x_j \partial x_k} + \sum_i \frac{\partial}{\partial x_i}\frac{\partial^2 L}{\partial x_j \partial x_k} f^i(\bar{x},t) \\ &+ \sum_i \left[\frac{\partial^2 L}{\partial x_i \partial x_j}\frac{\partial f^i}{\partial x_k} + \frac{\partial^2 L}{\partial x_i \partial x_k}\frac{\partial f^i}{\partial x_j} + \frac{\partial L}{\partial x_i}\frac{\partial^2 f^i}{\partial x_j \partial x_k}\right] \\ &= \frac{\partial^2 r}{\partial x_j \partial x_k} \end{aligned} \tag{14}$$

Using $(\dot{})$ for the characteristic derivative, this becomes

$$\begin{aligned} &\frac{\partial^2 \dot{L}}{\partial x_j \partial x_k} + \sum_i \left[\frac{\partial^2 L}{\partial x_i \partial x_j}\frac{\partial f^i}{\partial x_k} + \frac{\partial^2 L}{\partial x_i \partial x_k}\frac{\partial f^i}{\partial x_j} + \frac{\partial L}{\partial x_i}\frac{\partial^2 f^i}{\partial x_j \partial x_k}\right] \\ &= \frac{\partial^2 r}{\partial x_j \partial x_k} \end{aligned} \tag{15}$$

The initial value of $\partial^2 L/\partial x_j \partial x_k$, which is obtained from Eq. (9), is

$$\frac{\partial^2 L}{\partial x_j \partial x_k} = S \tag{16}$$

Note that the terms in Eq. (14) depend upon $\partial L/\partial x_i$, $\partial^2 L/\partial x_i \partial x_j$, $\bar{x}$, and known functions. Hence, the combined initial value problem defined by Eqs. (10), (12), (13), (14), and (15) is complete and well defined. This technique may be used to compute higher derivatives of L.

In each case a complete set of characteristic equations will be obtained.

The method of approximation consists of employing a finite number of terms in the expansion of $L(x, t)$ around $\bar{x}(t)$. If the first two terms are employed, then the approximation to the density function is the Gaussian density function

$$P(x,t) = K \exp\left[-1/2\,(x - x^*)^T \frac{\partial^2 L}{\partial x^2}\,(x - x^*)\right] \tag{17}$$

when

$$x^* = \bar{x} - \left(\frac{\partial^2 L}{\partial x^2}\right)^{-1} \frac{\partial L}{\partial x} \tag{18}$$

This should be a good approximation to the actual solution in the region if $||x - x^*||^2$ is small.

Note that for systems that conserve probability density ($r = 0$), $\partial L/\partial x = 0$. Hence, the approximate mean, or point of maximum density, lies along the original trajectory. In this case, $\partial^2 L/\partial x_i\,\partial x_j$ satisfies the characteristic equation

$$\frac{\partial^2 \dot{L}}{\partial x_i\,\partial x_j} = -\sum_k \left[\frac{\partial^2 \dot{L}}{\partial x_i\,\partial x_j}\frac{\partial f^k}{\partial x_j} + \frac{\partial^2 L}{\partial x_i\,\partial x_j}\frac{\partial f^k}{\partial x_i}\right]$$

This is the same result that would be obtained by linearizing the equations around the nominal trajectory and then applying the continuity equation to solve the linearized problem exactly.

Reference

1. Schubart, J., "Numerische Aufsuchung Periodischer Losungen im Dreikorperproblem," *Astronomische Nachrichten*, Band 283, pp. 17–22, 1958.